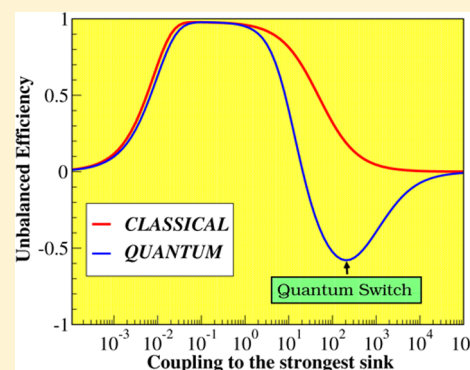


## Quantum Biological Switch Based on Superradiance Transitions

D. Ferrari,<sup>†</sup> G.L. Celardo,<sup>†,‡</sup> G.P. Berman,<sup>§</sup> R.T. Sayre,<sup>||</sup> and F. Borgonovi<sup>\*,†,‡</sup><sup>†</sup>Department of Mathematics and Physics and Interdisciplinary Laboratories for Advanced Materials Physics, Catholic University of Sacred Heart, via Musei 41, 25121 Brescia, Italy<sup>‡</sup>Istituto Nazionale di Fisica Nucleare, Sez. di Pavia, via Bassi 6, I-27100 Pavia, Italy<sup>§</sup>Theoretical Division, MS-B213, Los Alamos National Laboratories, Los Alamos, New Mexico 87545, United States<sup>||</sup>Los Alamos National Laboratory and New Mexico Consortium, 100 Entrada Drive, Los Alamos, New Mexico 87544, United States

## Supporting Information

**ABSTRACT:** A linear chain of connected sites with two asymmetric sinks, one attached to each end, is used as a simple model of quantum (excitonic and/or electron) transport in photosynthetic biocomplexes. For a symmetric initial population in the middle of the chain, it is expected that transport is mainly directed toward the strongly coupled sink. However, we show that quantum effects radically change this intuitive “classical” mechanism so that transport can occur through the weakly coupled sink with maximal efficiency. Using this capability, we show how to design a quantum switch that can transfer energy or charge to the strongly or weakly coupled branch of the chain, by changing the coupling to the sinks. The operational principles of this quantum device can be understood in terms of superradiance transitions and subradiant states. This switching, being a pure quantum effect, can be used as a witness of wavelike behavior in molecular chains. When realistic data are used for the photosystem II reaction center, this quantum biological switch is shown to retain its reliability, even at room temperature.



## INTRODUCTION

Understanding how biological systems transfer and store energy is a basic energy science challenge that can lead the design of new bionanotechnological devices.<sup>1–5</sup>

Recent experiments on photosynthesis by several groups<sup>6–14</sup> have suggested the striking role of quantum coherence in the form of long lasting oscillations of the population of excitonic states in light harvesting complexes (LHC), at room temperature. Despite these experimental findings there is no general consensus on the role quantum coherence plays in energy and/or electron transfer efficiency ( $\approx 99\%$ ).<sup>15–20</sup> For this reason exploration of the consequences of quantum coherence in biological nanodevices is one of the main interests in the novel field of quantum biology.

Here we analyze quantum transport inspired by the photosystem II (PSII) Reaction Center (RC) of many bacteria, plants, and algae, where the primary charge separation occurs. The RC is arranged in two symmetric branches, even if only one of them is active for the electron transport. Different mechanisms which could be responsible for the asymmetry in the PSII RCs and the related experiments are discussed in refs 21–30 (see also references therein).

Here we do not address the question why only one branch is active, but we use the PSII RC as a prototype for an artificial biological switch, able to drive energy or electron transport to the strongly or the weakly coupled branch, by controlling the couplings to the sinks.

Primary charge separation in the RC can be modeled starting from a donor (a dimer, called the special pair where the excitation starts) and then including different protein subunits, (bacterio) chlorophylls, and (bacterio) pheophytins, generally called chromophores.<sup>26–33</sup> While there exists much experimental data for calculating both the energy levels and the couplings between the chromophores, our aim here is to avoid nonessential technicalities which complicate the model and concentrate on the main ideas of designing a quantum switching device based on the PSII RC by attaching each end point of the branch to two sinks through which the electron or energy can escape the system (see Figure 1).

Models of transport in open quantum systems can be described within the framework of an effective non-Hermitian Hamiltonian which takes into account the loss of probability to the sinks. The presence of sinks can induce superradiance transitions (ST), which strongly affect transport properties. Note that in biosystem superradiance has been considered mainly as an effect of the coupling with the electromagnetic field,<sup>34</sup> but actually it is a generic effect<sup>35</sup> which can occur whenever a system is coupled to a continuum of states. The superradiant effect, considered here, is induced by the coupling to a continuum of scattering states characterizing the sinks. It is

Received: July 4, 2013

Revised: December 10, 2013

Published: December 16, 2013

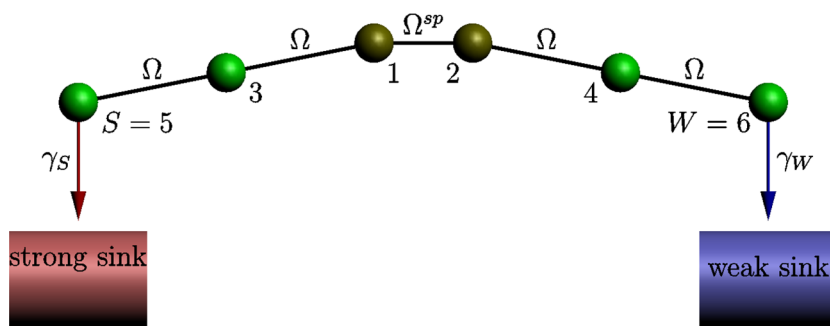


**Figure 1.** Multimer model for the PSII RC. The six sites have equal energies,  $E_0 = 0$ , and equal coupling constants,  $\Omega$ . The pair 1–2 is characterized by the coupling constant,  $\Omega^{sp} > \Omega$ . Left and right ends of the chain are connected, respectively, to the strongly and weakly coupled sink by the coupling constants,  $\gamma_S$  and  $\gamma_W$ , that represent couplings to two different continuum electron environments.

also related to the supertransfer phenomenon discussed in ref 36, and it has been analyzed in different contexts<sup>35,37–40</sup> for the case of one sink or two identical sinks and in ref 41 for the case of two asymmetrical sinks in the context of transport through a sequence of one-dimensional potential barriers. To the best of our knowledge, the intrinsic mechanism of superradiance and its relation to energy and electron transport has not been fully understood in biosystems. Here we show how superradiant transitions can induce a switching of transport, which is a pure quantum coherent effect.

## ■ THE MODEL

The model we consider consists of six sites divided into two symmetric branches with two independent sinks attached at the ends. For simplicity, the energies of the sites are taken to be equal,  $E_0 = 0$ , and the coupling between the nearest-neighbor sites is constant ( $\Omega$ ). The central pair of sites is allowed to have a larger coupling constant,  $\Omega^{sp} > \Omega$ . This very simple system was considered in the literature (called the “multimer” model<sup>42,43</sup>) as a prototype model for the PSII RC and is shown schematically in Figure 1. Despite its simplicity (currently more complicated models have been introduced<sup>44,45</sup>), we believe it contains the essence of the process we are modeling. Later, in Sections III and IV, we will show that the results which follow from our model maintain their validity in a large range of parameters when more realistic models and thermal effects are taken into account.

The asymmetry in our model arises only from the different coupling strengths with the sinks, which can be understood as representing continuum electron energy spectra. These electron environments are characterized by the transition rates to the strongly and to the weakly coupled branch of the system. We also choose symmetric initial conditions for sites 1 and 2

$$\rho(0) = \frac{1}{2}(|1\rangle + |2\rangle)(\langle 1| + \langle 2|) \quad (1)$$

(Similar results, not shown here, can be obtained for the symmetric mixed state described by a density matrix,  $\rho(0) = (1/2)(|1\rangle\langle 1| + |2\rangle\langle 2|)$ .)

An effective non-Hermitian Hamiltonian can be constructed as in ref 39 by coupling the system to two different continuum electron reservoirs. The probability flow into these continua is analyzed with an effective non-Hermitian Hamiltonian,  $\mathcal{H}$

$$\mathcal{H} \equiv H_0 - i\frac{\gamma_S}{2}W_S - i\frac{\gamma_W}{2}W_W = \begin{pmatrix} 0 & \Omega^{sp} & \Omega & 0 & 0 & 0 \\ \Omega^{sp} & 0 & 0 & \Omega & 0 & 0 \\ \Omega & 0 & 0 & 0 & \Omega & 0 \\ 0 & \Omega & 0 & 0 & 0 & \Omega \\ 0 & 0 & \Omega & 0 & -i\gamma_S/2 & 0 \\ 0 & 0 & 0 & \Omega & 0 & -i\gamma_W/2 \end{pmatrix} \quad (2)$$

where  $H_0$  is the Hamiltonian of the closed system, and  $W_{S,W}$  takes into account the coherent dissipation. As one can see, in the site basis this corresponds to adding imaginary terms to the end sites,  $|S\rangle$  and  $|W\rangle$ , describing the loss of electron probability to the sinks.

The eigenvalues of  $\mathcal{H}$  are complex numbers,  $E^{(k)} - i\Gamma^{(k)}/2$ , where  $\Gamma^{(k)}$  is the decay width and the evolution is described by the von Neumann equation<sup>39,46</sup>

$$\frac{d\rho}{dt} = -\frac{i}{\hbar}(\mathcal{H}\rho - \rho\mathcal{H}^\dagger) \quad (3)$$

We also introduce the parameters  $\kappa_{S(W)}$  and  $q$

$$\kappa_{S(W)} \equiv \frac{\gamma_{S(W)}}{2\Omega}, \quad q \equiv \frac{\kappa_S}{\kappa_W} \quad (4)$$

and the efficiencies of transport to the sinks through the strongly ( $|S\rangle$ ) and the weakly coupled ( $|W\rangle$ ) site) branch during the time,  $T$

$$\eta_{S(W)}(T) = \frac{\gamma_{S(W)}}{\hbar} \int_0^T dt \langle S(W)|\rho(t)|S(W)\rangle \quad (5)$$

As shown in ref 41, two superradiant transitions with the corresponding formation of two superradiant (SR) states are expected to occur at

$$\begin{cases} (ST_S) & \frac{\gamma_S}{2\Omega} \simeq 1, \Rightarrow \kappa_S \simeq 1 \\ (ST_W) & \frac{\gamma_W}{2\Omega} \simeq 1, \Rightarrow \kappa_S \simeq q \end{cases} \quad (6)$$

Strictly speaking, in ref 41 the STs have been found to agree with eq 6 under the conditions of a very large number of sites,  $N \gg 1$ , and  $\Omega^{sp} = \Omega$ . We checked that eq 6 is a good estimate for the STs even for small  $N$  values and in a large range of  $\Omega^{sp} \neq \Omega$ .

Let us analyze the physical picture in which STs can be seen. A small coupling with the continuum typically produces level broadening; that is, all levels equally acquire a width proportional to the opening strength. This “perturbative” argument is valid up to a critical strength: when the widths of neighboring levels overlap a “segregation” occurs. In other words, one energy level continues to have a width proportional to the opening (SR state), while all other levels (subradiant states) are characterized by a decay width inversely proportional to the opening strength. This sharp transition has been called superradiant transition, in analogy with the Dicke superradiance, since the SR state owns a width  $N$  times larger than the average width (if  $N$  is the number of levels), and it decays  $N$  times faster than the other states. On the contrary, the subradiant states, in the limit of very large opening strength, lose their widths and do not decay at all.

The above general picture holds also in the presence of asymmetric couplings with two different sinks, as shown in ref 41. Indeed, increasing  $\kappa_S$  at fixed  $q$  produces two STs that can be observed by two peaks in the average width of the  $N - 2$  subradiant states (see Figure 2a).

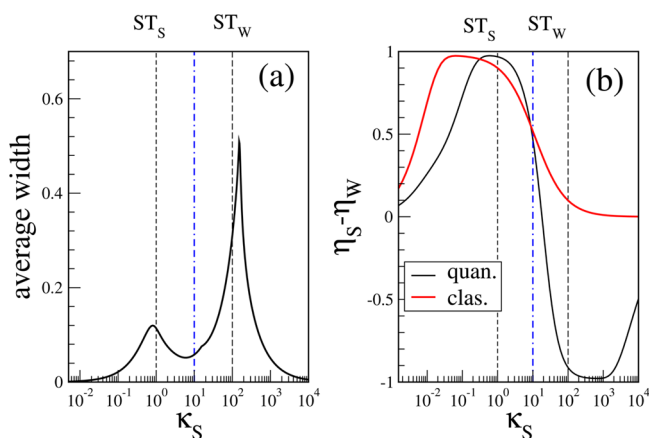


**Figure 2.** (a) Average energy width of the  $N - 2$  eigenstates which do not become superradiant as a function of the effective coupling strength,  $\kappa_S$ , at fixed  $q = \kappa_S/\kappa_W = 100$ . Average width has also been normalized by the average energy distance between levels,  $D \simeq \Omega$ . (b) Unbalanced efficiency,  $\eta_S - \eta_W$ , as a function of the effective coupling strength,  $\kappa_S$ , for the quantum case (black lower) and for the classical case (red upper). Here  $\Omega = 100 \text{ cm}^{-1}$  and  $\Omega^{\text{sp}} = 200 \text{ cm}^{-1}$ . The efficiencies have been obtained by integrating over  $T = 20 \text{ ps}$ . In both panels, the vertical dashed lines represent, respectively, the strong and the weak STs, while the dashed-dotted central line indicates the switching line (see text below).

We now discuss the efficiency of transport to the sinks under the condition that the coupling to the strongly coupled sink,  $\gamma_S$ , is always larger than the coupling to the weakly coupled one,  $\gamma_W$ . One might expect that the sink with the strong coupling (stronger probability per unit of time to escape the chain) will be the most efficient, but what happens in this quantum system is more complicated. Indeed, Figure 2b shows that the unbalanced efficiency,  $\eta_S - \eta_W$ , as a function of the coupling strength,  $\kappa_S$ , takes almost all values between  $-1$  and  $1$ , with two maxima close to the STs. In other words, close to the strong ST ( $ST_S$ ,  $\kappa_S \simeq 1$ ), the efficiency has a maximum through the strongly coupled branch ( $\eta_S \simeq 1$ ,  $\eta_W \simeq 0$ ), while close to the weak ST ( $ST_W$ ,  $\kappa_S \simeq q$ ), the efficiency has a maximum through the weakly coupled branch ( $\eta_S \simeq 0$ ,  $\eta_W \simeq 1$ ). This is an unexpected

result since the whole picture has been obtained under the condition  $\kappa_S \gg \kappa_W$ , namely, at the fixed ratio,  $q = \kappa_S/\kappa_W = 100 \gg 1$ .

Therefore, the whole system can act as a probability switch even in the presence of a strong different coupling between the two branches. How is this possible? Before explaining these results and their intrinsic quantum nature, we consider the “classical” behavior of this model. The classical dynamics can be modeled considering an incoherent hopping among the sites, thus described by a classical Pauli master equation with coupling among diagonal density matrix elements only (populations)

$$\frac{d\rho_{ii}}{dt} = \sum_k (T_{ik}\rho_{kk} - T_{ki}\rho_{ii}) - \left( \frac{\gamma_S}{\hbar}\delta_{Si} + \frac{\gamma_W}{\hbar}\delta_{Wi} \right) \rho_{ii} \quad (7)$$

where  $\rho_{ii}$  is the probability at the  $i$ -th site;  $T_{ik} = (H_0)_{ik}/\hbar$  is the transition rate from the  $k$ -th to the  $i$ -th sites; and the last two terms represent the flow of probability through the strong ( $S$ ) and weak ( $W$ ) sinks.

The results of the classical dynamics, for the same model and symmetric initial conditions,  $\rho_{11}(0) = \rho_{22}(0) = 1/2$ , are shown in Figure 2b (red curve). They demonstrate the absence of a switch of transmission from the strongly to the weakly coupled branch. Indeed, one always finds  $\eta_S > \eta_W$  and  $\eta_S \simeq \eta_W \simeq 1/2$  for large values of  $\kappa_S$ . Up to some extent, this is in agreement with an intuitive interpretation: if the coupling strengths to both sinks are extremely strong, particles will be absorbed by both sinks with the same efficiency. We can use these results to define “classical transport” as one occurring through the strongly coupled branch and “quantum transport” as one occurring through the weaker coupled branch.

These results immediately raise the following two questions: How can it happen that the transport occurs through the weaker coupled branch? Is it possible to estimate analytically the “switching point”,  $\kappa_S^{\text{sw}}$ , located between the two STs at which  $\eta_S \simeq \eta_W$ ?

To answer both questions, we investigated the structure (localization and decay width) of the eigenfunctions of the effective non-Hermitian Hamiltonian. In the region between the two STs where the switching occurs, there is only one SR state. Even if its width is very large, it becomes strongly localized around the strong sink, leaving the other subradiant states approximately extended with no overlap with the strong sink (see the Supporting Information). This mechanism stops the transport through the strongly coupled branch and simultaneously induces the transport through the weakly coupled branch.

Let us analytically estimate the critical value,  $\kappa_S^{\text{sw}}$ , at which the switching from the strongly to the weakly coupled branch occurs. Assuming that the switching occurs when the partial decay widths to the strong,  $\Gamma_S$ , and to the weak,  $\Gamma_W$ , are equal, and since between the two STs,  $\Gamma_S \propto 1/\kappa_S$  and  $\Gamma_W \propto \kappa_S/q$  (see Supporting Information and ref 47) one gets

$$\frac{1}{\kappa_S} \simeq \frac{\kappa_S}{q} \Rightarrow \kappa_S^{\text{sw}} \simeq \sqrt{q} \quad (8)$$

When the condition 8 is met, the unbalanced efficiency is approximately zero. This is verified directly in Figure 2b, where the theoretical dashed-dotted vertical line,  $\kappa_S^{\text{sw}} \simeq \sqrt{q}$ , is in a good agreement with the switching point at which the unbalanced efficiency becomes zero. Note that in our case

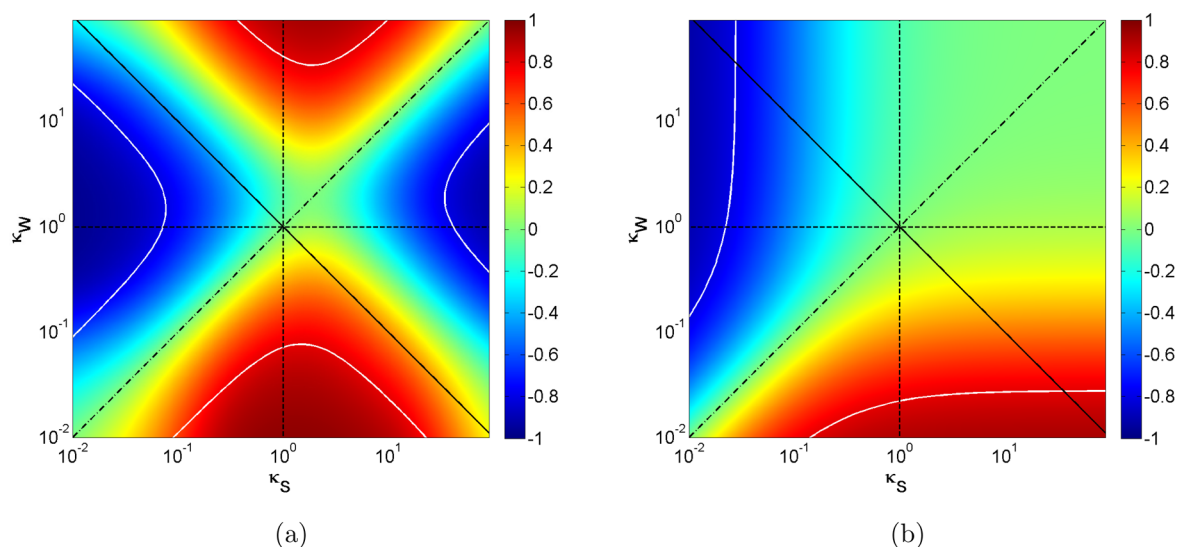


**Figure 3.** Two-dimensional contour plot,  $\eta_S - \eta_W$ , as a function of  $\kappa_S = \gamma_S/2\Omega$  and  $\kappa_W = \gamma_W/2\Omega$  in log–log scale for the quantum (a) and the classical case (b). The vertical and horizontal lines are, respectively, the  $ST_S$  and  $ST_W$ . The two diagonals are the symmetry line  $\kappa_S = \kappa_W$  (dashed) and the switching line  $\kappa_S = 1/\kappa_W$  (full). White curves represent 90% of the ratio between the two efficiencies ( $\eta_S/\eta_W = 9$  or  $\eta_W/\eta_S = 9$ ).

the same condition in eq 8 also defines the minimal decay width between the two STs (see Figure 2a).

One could ask whether these results are due to the strong asymmetry ( $q = 100$ ) used above. The negative answer can be extracted from the “phase diagram” of Figure 3, in which the unbalanced efficiency is shown for all values of  $\kappa_S$  and  $\kappa_W$  and for both the quantum case (left panel) and the classical case (right panel), where the regions of transport to the strongly coupled branch have been indicated by red color and the transport to the weakly coupled branch by the blue color. While the classical picture shows that switching between the red and the blue regions is possible only crossing the symmetry line,  $\kappa_S = \kappa_W$ , in the quantum world a further possibility is given by crossing the curve,  $\kappa_S = 1/\kappa_W$ .

### EFFICIENCY OF THE TRANSPORT IN THE PRESENCE OF A THERMAL BATH

The presence of a thermal bath can strongly influence transport properties;<sup>48,49</sup> for this reason, to demonstrate the robustness of the approach described above, we consider the interaction of our system with a phonon bath at finite temperature. We use the thermal bath as in ref 48 whose dynamics is described by the Lindblad master equation in the Born–Markov and secular approximations. More realistic models for the thermal bath can be found in the literature.<sup>44,45</sup> This simpler approach has already been used to describe the FMO complex in a very similar framework.<sup>39,48</sup> Note that this approach leads to the relaxation of the populations,  $\rho_{kk}$  to Gibbs distribution.

We use the Lindblad-type master equation in the form

$$\frac{d\rho}{dt} = -\frac{i}{\hbar}(\mathcal{H}\rho - \rho\mathcal{H}^\dagger) + L_p(\rho) \quad (9)$$

where the action of the Lindblad operator,  $L_p(\rho)$ , on  $\rho$  is described by eq 5 of ref 48 (see Supporting Information). In particular, we choose an exponential spectral density dependent on two parameters, the reorganization energy,  $E_R$ , and the cutoff frequency,  $\omega_c$ , to be considered together with the temperature,  $T$ , of the bath.

The thermal bath (interaction with phonons) produces an homogeneous line broadening,<sup>50</sup>  $\gamma_T$ , proportional to both

temperature and reorganization energy and inversely proportional to the cutoff frequency<sup>51</sup>

$$\gamma_T = 2\pi \left( \frac{kT}{\hbar} \right) \left( \frac{E_R}{\hbar\omega_c} \right) \quad (10)$$

In Figure 4, we plot the unbalanced efficiency as a function of the coupling,  $\kappa_S$ , at  $T = 300$  K and reorganization energy and

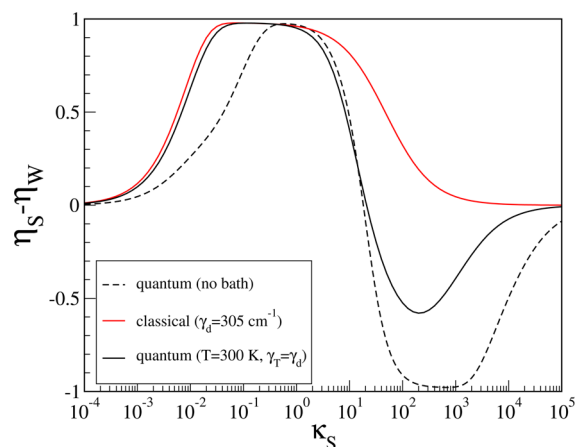


**Figure 4.** Effects of a thermal bath. Unbalanced efficiency,  $\eta_S - \eta_W$ , as a function of the effective coupling strength,  $\kappa_S$ . Black full line stands for quantum transport in the presence of a thermal bath at  $T = 300$  K,  $\omega_c = 150$   $\text{cm}^{-1}$ , and  $E_R = 35$   $\text{cm}^{-1}$ , so to have a homogeneous line broadening  $\gamma_T = 305.7$   $\text{cm}^{-1}$ . Dashed line is the quantum calculation done before (microcanonical). Red line stands for the classical master equation eq 7, with the semiclassical rates, eq 10, and  $\gamma_d = \gamma_T = 305.7$   $\text{cm}^{-1}$ . Here  $\Omega = 100$   $\text{cm}^{-1}$ ,  $\Omega^{\text{sp}} = 200$   $\text{cm}^{-1}$ , and  $q = \kappa_S/\kappa_W = 100$  fixed. Strong and weak efficiencies have been obtained by integrating over 20 ps.

cutoff frequency chosen to have a homogeneous line broadening  $\gamma_T = 305.7$   $\text{cm}^{-1}$  (full black curve).

As one can see, the first effect is that the quantum switching due to the superradiance is weakened but not suppressed by the thermal bath (compare with the dashed curve which represents

the same quantity in the absence of the thermal bath for the same value of  $q = \kappa_S/\kappa_W = 100$ ).

To have a close comparison with the classical model we consider the same classical master equation as before, eq 7, but with the transition rates, computed semiclassically as in refs 39 and 50

$$T_{ik} = \frac{2\Omega_{ik}^2}{\hbar\gamma_d} \left( 1 + \frac{\Delta E_{ik}^2}{\gamma_d^2} \right)^{-1} \quad (11)$$

where  $\Omega_{ik}$  represents the energy coupling between the  $i$ -th and the  $k$ -th sites; the  $\Delta E_{ik}$  are the energy differences between the two sites; and  $\gamma_d$  is the dephasing energy.<sup>50</sup>

To have a close comparison we put the dephasing energy  $\gamma_d = \gamma_T$ . Results obtained from the classical master equation with the semiclassical rates in eq 11 are shown in Figure 4 as a red curve.

As one can see, the switching is absent in the classical model since the incoherent hopping transport gives at most  $\eta_W \approx \eta_S \approx 1/2$ . The most interesting result is that the presence of the thermal bath has the opposite effects on classical and quantum transport: the thermal bath weakens only the quantum transport (transport to the weakly coupled branch), while it leaves mainly unaffected the classical transport (strongly coupled branch). The different sensibility of transport to the dephasing induced by the thermal bath is consistent with the quantum coherent nature of the switch. This fact opens the interesting possibility to detect experimentally the dephasing due to the phonon bath and the degree of quantum coherence in nanoscopic devices by measuring the efficiency through the weakly coupled sink. Indeed, given a molecular network we can couple the system to two external leads, and we can control the coupling strength by varying the tunneling coupling,  $V$ , to the external leads or their density of states,  $\rho$ , since from the Fermi golden rule  $\gamma = 2\pi V^2 \rho$  (see also refs 40 and 41).

This opens the interesting possibility to use the switch effect as a witness of quantum coherence in molecular chains.

## EFFICIENCY FOR A REALISTIC MODEL

Here we apply our approach to a realistic model<sup>52</sup> of the photosystem II reaction center (PSII RC). This system has eight chromophores in the left–right subunits: two chlorophylls belonging to the central special pair, two accessory chlorophylls, two pheophytins, and two peripheral chlorophylls, not relevant since weakly coupled. To match 2D spectroscopy data, the energy levels in the active branch (strongly coupled) are not the same as for the inactive branch (weakly coupled) and range between 15 000 and 15 555  $\text{cm}^{-1}$ . Moreover, the coupling constants among chromophores are not equal for nearest neighbors, and all chromophores couple to each other with strengths varying from 0.12 to 162.2  $\text{cm}^{-1}$ . The exact Hamiltonian matrix is not presented here, but it can be found in ref 52. Due to many differences from the simple model discussed above, one can wonder whether the previously discussed switching effect persists in this realistic model characterized by nondegenerate energy levels, long-range interactions, and absence of exact left–right symmetry.<sup>52</sup>

We proceed as before, by attaching the sinks to the pheophytins, designing the effective non-Hermitian Hamiltonian, and calculating the conditions for the strong and the weak STs (computed from the complex eigenvalues of the non-Hermitian Hamiltonian of this model, indicated as dashed vertical lines in Figure 5c). As one can see, the maximal strong/

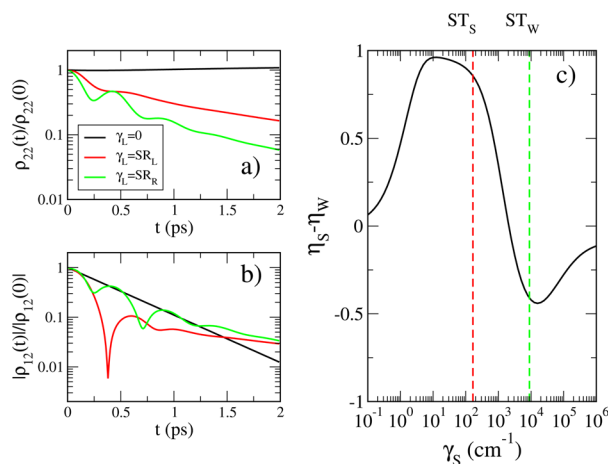


**Figure 5.** Realistic model of a RC. Left panels: (a) Decay of populations in time. (b) Decay of coherences in time for fixed ratio,  $q = \gamma_S/\gamma_W = 100$ , and different values of  $\gamma_S$ , as indicated in the legend. Right panel: (c) Unbalanced average efficiency,  $\eta_S - \eta_W$ , as a function of the effective coupling strength,  $\gamma_S$ , for 300 K. A reorganization energy,  $E_R = 20 \text{ cm}^{-1}$ , and cutoff frequency,  $\omega_c = 150 \text{ cm}^{-1}$ , have been chosen to have an approximate decay of populations and coherences on the time scale of 1 ps. See left panels (a) and (b).

weak efficiency roughly peaks near the  $\text{ST}_{S,W}$  ( $\text{ST}_{S,W}$  values for this model have been obtained by numerical diagonalization of the effective Hamiltonian).

To show that the switch can work at room temperature, we embedded the system in a thermal bath as described above. We note that the bath considered in eq 9, without sinks, produces in the secular approximations uncoupled equations for populations (diagonal matrix elements) and coherences (off-diagonal ones) in the energy basis.<sup>33</sup> In particular, for excitonic dynamics, populations relax in time to Gibbs distribution without oscillations, at variance with the experiment.<sup>6–14</sup> For purely electronic dynamics, the role of coherences has been less studied. For a recent discussion about electronic coherences in the reaction centers of *Rhodobacter sphaeroides*, see ref 53.

Nevertheless, due to the non-Hermitian term, a coupling between populations and coherences appears. The effect of the dynamics generated by the sinks is shown in Figure 5a,b, in which oscillations are clearly observable for  $\gamma_S \neq 0$ , showing that coherences and populations are now coupled.

We therefore use the same thermal bath as in eq 9, setting the parameters for reorganization energy,  $E_R$ , and cutoff frequency,  $\omega_c$ , to have a decay of both populations and coherences of the order of 1 ps, in agreement with experiments.<sup>13</sup> Our results (shown in Figure 5c) demonstrate that the previously observed switching survives in the presence of a thermal bath at room temperature (even though it reduces the unbalanced efficiency to the weakly coupled branch,  $\approx 0.5$ , compared with the strongly coupled one,  $\approx 1$ ). Note that for the realistic system maximal efficiency occurs at  $\gamma_S = 10 \text{ cm}^{-1}$ , which corresponds to a coupling rate of  $2 \text{ ps}^{-1}$ .

## CONCLUSIONS

The analysis of our model for exciton or electron transport, consisting of two branches attached to two asymmetric sinks, revealed two different transport regimes: a classical one, in which transport occurs through the strongly coupled sink, and a quantum one, in which transport occurs through the weakly coupled sink. Varying the coupling strengths in an appropriate

way (see Figure 3a), one can switch from one regime to the other, thus inducing a switching of transport from one branch to the other. This switching is a pure quantum effect, based on the existence of two consecutive superradiance transitions as the couplings vary. The quantum nature of the switching is confirmed by the analysis of the coupling to a thermal bath: only quantum transport is weakened by the thermal bath, not the classical one.

Even if in this paper we did not suggest any specific experiment, we think that the switching effect could be useful to measure the amount of quantum coherence in the molecular network and different experimental setups. For instance, apart from the example discussed in the paper, one of the systems relevant to our model could be a light harvesting complex (LHC) interacting with different reaction centers (sinks) (see for instance ref 54). In this case, the LHC has a very complex structure/geometry, and it is connected with two (or more) RCs. These connections can be described by the interactions of the LHC with many sinks, as in our model. By modifying the interaction constants (by mutation technique) one can realize simultaneously both weak and strong interactions of the LHC with two sinks. So, the exciton transport can be adequately described by our model. In this case, the quantum switching effect based on the ST could be realized and observed in this system. We plan to follow this direction in a future work.

## ■ ASSOCIATED CONTENT

### Supporting Information

Additional experimental details and figures. This material is available free of charge via the Internet at <http://pubs.acs.org>.

## ■ AUTHOR INFORMATION

### Corresponding Author

\*E-mail: [fausto.borgonovi@unicatt.it](mailto:fausto.borgonovi@unicatt.it).

### Notes

The authors declare no competing financial interest.

## ■ ACKNOWLEDGMENTS

This work has been supported by Regione Lombardia and CILEA Consortium through a LISA Initiative (Laboratory for Interdisciplinary Advanced Simulation) 2011 grant available at <http://lisa.cilea.it>. Support by the grant D.2.2 2011 (Calcolo ad alte prestazioni) from Università Cattolica is also acknowledged. The work by GPB and RTS was carried out under the auspices of the National Nuclear Security Administration of the U.S. Department of Energy at Los Alamos National Laboratory under Contract No. DE-AC52-06NA25396. We also thank Gary Doolen for useful comments.

## ■ REFERENCES

- (1) Barber, J. Photosynthetic energy conversion: natural and artificial. *Chem. Soc. Rev.* **2009**, *38*, 185–196.
- (2) Tachibana, Y.; Vayssieres, L.; Durrant, J. R. Artificial photosynthesis for solar water-splitting. *Nat. Photonics* **2012**, *6*, 511–518.
- (3) Valov, I.; Linn, E.; Tappertzhofen, S.; Schmelzer, S.; van den Hurk, J.; Lentz, F.; Waser, R. Nanobatteries in redox-based resistive switches require extension of memristor theory. *Nature Commun.* **2013**, *4*, 1771.
- (4) Smirnov, A.; Mouroukh, L. G.; Ghosh, P. K.; Nori, F. High-Efficiency Energy Conversion in a Molecular Triad Connected To Conducting Leads. *J. Phys. Chem. C* **2009**, *113*, 21218–21224.
- (5) Carrara, S. Nano-bio-technology and sensing chips: new systems for detection in personalized therapies and cell biology. *Sensors* **2010**, *10*, 526–543.
- (6) Hu, X.; Damjanovich, A.; Ritz, T.; Schulten, K. Architecture and mechanism of the light-harvesting apparatus of purple bacteria. *J. Phys. Chem. B* **1997**, *101*, 3854–3871.
- (7) Brixner, T.; Stenger, J.; Vaswani, H. M.; Cho, M.; Blankenship, R. E.; Fleming, G. R. Two-dimensional spectroscopy of electronic couplings in photosynthesis. *Nature* **2005**, *434*, 625–628.
- (8) Lee, H.; Cheng, Y.-C.; Fleming, G. R. Coherence dynamics in photosynthesis: protein protection of excitonic coherence. *Science* **2007**, *316*, 1462–1465.
- (9) Engel, G. S.; Calhoun, T. R.; Read, E. L.; Ahn, T. K.; Man, T.; Cheng, Y. C.; Blankenship, R. E.; Fleming, G. R. Evidence for wavelike energy transfer through quantum coherence in photosynthetic systems. *Nature* **2007**, *446*, 782–786.
- (10) Raszewski, G.; Diner, B. A.; Schlodder, E.; Renger, T. Spectroscopic properties of reaction center pigments in photosystem II core complexes: revision of the multimer model. *Biophys. J.* **2008**, *95*, 105–119.
- (11) Panitchayangkoon, G.; Hayes, D.; Fransted, K. F.; Caram, J. R.; Harel, E.; Wen, J.; Blankenship, R. E.; Engel, G. S. Long-lived quantum coherence in photosynthetic complexes at physiological temperature. *Proc. Natl. Acad. Sci. U.S.A.* **2010**, *107*, 12766–12770.
- (12) Collini, E.; Wong, C. Y.; Wilk, K. E.; Curmi, P. M. G.; Brumer, P.; Scholes, G. D. Coherently wired light-harvesting in photosynthetic marine algae at ambient temperature. *Nature* **2010**, *463*, 644–647.
- (13) Westenhoff, S.; Palecek, D.; Edlund, P.; Smith, P.; Zigmantas, D. Coherent picosecond exciton dynamics in a photosynthetic reaction center. *J. Am. Chem. Soc.* **2012**, *134*, 16484–16487.
- (14) Wong, C. Y.; Alvey, R. M.; Turner, D. B.; Wilk, K. E.; Bryant, D. A.; Curmi, P. M. G.; Silbey, R. J.; Scholes, G. D. Electronic coherence lineshapes reveal hidden excitonic correlations in photosynthetic light harvesting. *Nature Chem.* **2012**, *4*, 396–404.
- (15) Ishizaki, A.; Fleming, G. R. Theoretical examination of quantum coherence in a photosynthetic system at physiological temperature. *Proc. Natl. Acad. Sci. U.S.A.* **2009**, *106*, 17255–17260.
- (16) Cheng, Y.-C.; Fleming, G. R. Dynamics of light harvesting in photosynthesis. *Annu. Rev. Phys. Chem.* **2009**, *60*, 241–262.
- (17) Scholes, G. D.; Fleming, G. R.; Olaya-Castro, A.; van Grondelle, R. Lessons from nature about solar light harvesting. *Nature Chem.* **2011**, *3*, 763–774.
- (18) Strumpfer, J.; Sener, M.; Schulten, K. How quantum coherence assists photosynthetic light-harvesting. *J. Phys. Chem. Lett.* **2012**, *3*, 536–542.
- (19) Dawlaty, J. M.; Ishizaki, A.; De, A. K.; Fleming, G. R. Microscopic quantum coherence in a photosynthetic-light-harvesting antenna. *Philos. Trans. R. Soc. A* **2012**, *370*, 3672–3691.
- (20) Kassal, I.; Yuen-Zhou, J.; Rahimi-Keshari, S. Does coherence enhance transport in photosynthesis? *J. Phys. Chem. Lett.* **2013**, *4*, 362–367.
- (21) Scherer, P. O. J.; Fischer, S. F. Long-range electron transfer within the hexamer of the photosynthetic reaction center Rhodospseudomonas viridis. *J. Phys. Chem.* **1989**, *93*, 1633–1637.
- (22) Giorgi, L. B.; Nixon, P. J.; Merry, S. A. P.; Joseph, D. M.; Durrant, J. R.; De Las Rivas, J.; Barber, J.; Porter, G.; Klug, D. R. Comparison of Primary Charge Separation in the Photosystem II Reaction Center Complex Isolated from Wild-type and D1–130 Mutants of the Cyanobacterium *Synechocystis* PCC 6803. *J. Biol. Chem.* **1996**, *271*, 2093–2101.
- (23) Dorlet, P.; Xiong, L.; Sayre, R. T.; Un, S. High field EPR study of the pheophytin anion radical in wild type and D1-E130 mutants of photosystem II in *Chlamydomonas reinhardtii*. *J. Biol. Chem.* **2001**, *276*, 22313–22316.
- (24) Xiong, L.; Seibert, M.; Gusev, A. V.; Wasielewski, M. R.; Hemann, C.; Hille, C.; Sayre, R. T. Substitution of a chlorophyll into the inactive branch pheophytin-binding site impairs charge separation in photosystem II. *J. Phys. Chem. B* **2004**, *108*, 16904–16911.

- (25) Rappaport, F.; Cuni, A.; Xiong, L.; Sayre, R.; Lavergne, R.; Charge, J. recombination and thermoluminescence in photosystem II. *Biophys. J.* **2005**, *88*, 1948–1958.
- (26) Pincak, R.; Pudlak, M. Noise breaking the twofold symmetry of photosynthetic reaction centers: Electron transfer. *Phys. Rev. E* **2001**, *64*, 031906.
- (27) Pudlak, M. Primary charge separation in the bacterial reaction center: Validity of incoherent sequential model. *J. Chem. Phys.* **2003**, *118*, 1876.
- (28) Lakhno, V. D. Oscillations in the primary charge separation in bacterial photosynthesis. *Phys. Chem. Chem. Phys.* **2002**, *4*, 2246–2250.
- (29) Lakhno, V. D. Dynamical Theory of Primary Processes of Charge Separation in the Photosynthetic Reaction Center. *J. Biol. Phys.* **2005**, *31*, 145–159.
- (30) Pudlak, M.; Pincak, R. Electronic pathway in reaction centers from *Rhodobacter sphaeroides* and *Chloroflexus aurantiacus*. *J. Biol. Phys.* **2010**, *36*, 273–289.
- (31) Novoderezhkin, V. I.; Dekker, J. P.; van Grondelle, R. Mixing of exciton and charge-transfer states in photosystem II reaction centers: modeling of stark spectra with modified Redfield theory. *Biophys. J.* **2007**, *93*, 1293–1311.
- (32) Abramavicius, D.; Mukamel, S. Energy-transfer and charge-separation pathways in the reaction center of photosystem II revealed by coherent two-dimensional optical spectroscopy. *J. Chem. Phys.* **2010**, *133*, 184501.
- (33) Abramavicius, D.; Mukamel, S. Quantum oscillatory exciton migration in photosynthetic reaction centers. *J. Chem. Phys.* **2010**, *133*, 064510.
- (34) Spano, F. C.; Mukamel, S. , Superradiance in molecular aggregates. *J. Chem. Phys.* **1989**, *91*, 683–700. Monshouwer, R.; Abrahamsson, M. Van Mourik, F.; van Grondelle, R. Superradiance and Exciton Delocalization in Bacterial Photosynthetic Light-Harvesting Systems. *J. Phys. Chem. B* **1997**, *101*, 7241–7248.
- (35) Auerbach, N.; Zelevinsky, V. Super-radiant dynamics, doorways and resonances in nuclei and other open mesoscopic systems. *Rep. Prog. Phys.* **2011**, *74*, 106301–106335. Volya, A.; Zelevinsky, V. Conference Proceedings. *Nuclei and Mesoscopic Physics: WNMP 2004*; Zelevinsky, V., Ed.; AIP: Melville, 2005; Vol. 777, p 229.
- (36) Lloyd, S.; Mohseni, M. Symmetry-enhanced supertransfer of delocalized quantum states. *New J. Phys.* **2010**, *12*, 075020.
- (37) Celardo, G. L.; Kaplan, L. Superradiance transition in one-dimensional nanostructures: An effective non-Hermitian Hamiltonian formalism. *Phys. Rev. B* **2009**, *79*, 155108.
- (38) Toroker, M. C.; Peskin, U. On the relation between steady-state currents and resonance states in molecular junctions. *J. Phys. B: At, Mol. Opt. Phys.* **2009**, *42*, 044013.
- (39) Celardo, G. L.; Borgonovi, F.; Merkli, M.; Tsifrinovich, V. I.; Berman, G. P. Superradiance transition in photosynthetic light-harvesting complexes. *J. Phys. Chem. C* **2012**, *116*, 22105–22111.
- (40) Sadreev, A. F.; Rotter, I. S-matrix theory for transmission through billiards in tight-binding approach. *J. Phys. A* **2003**, *36*, 11413.
- (41) Celardo, G. L.; Smith, A. M.; Sorathia, S.; Zelevinsky, V. G.; Sen'kov, R. A.; Kaplan, L. Transport through nanostructures with asymmetric coupling to the leads. *Phys. Rev. B* **2010**, *82*, 165437.
- (42) Durrant, J. R.; et al. A multimer model for P680, the primary electron donor of photosystem II. *Proc. Natl. Acad. Sci. U.S.A.* **1995**, *92*, 4798–4802.
- (43) Leegwater, J. A.; Durrant, J. R.; Klug, D. R. Exciton equilibration induced by phonons: theory and application to PS II reaction centers. *J. Phys. Chem. B* **1997**, *101*, 7205–7210.
- (44) Palmieri, B.; Abramavicius, D.; Mukamel, S. Lindblad equations for strongly coupled populations and coherences in photosynthetic complexes. *J. Chem. Phys.* **2009**, *130*, 240512.
- (45) Ishizaki, A.; Fleming, G. R. On the Interpretation of Quantum Coherent Beats Observed in Two-Dimensional Electronic Spectra of Photosynthetic Light Harvesting Complexes. *J. Phys. Chem. B* **2011**, *115*, 6227–6233.
- (46) Mukamel, S. *Principles of Nonlinear Optics and Spectroscopy*; Oxford University Press: New York, 1995.
- (47) Celardo, G. L.; Biella, A.; Kaplan, L.; Borgonovi, F. Interplay of superradiance and disorder in the Anderson model. *Fortschr. Phys.* **2013**, *61*, 250–260.
- (48) Mohseni, M.; Rebertrost, P.; Lloyd, S.; Aspuru-Guzik, A. Environment-assisted quantum walks in photosynthetic energy transfer. *J. Chem. Phys.* **2008**, *129*, 174106.
- (49) Plenio, M. B.; Huelga, S. F. Dephasing-assisted transport: quantum networks and biomolecules. *New J. Phys.* **2008**, *10*, 113019.
- (50) Leegwater, J. A. Coherent versus incoherent energy transfer and trapping in photosynthetic antenna complexes. *J. Phys. Chem.* **1996**, *100*, 14403–14409.
- (51) Rebertrost, P.; Mohseni, M.; Kassal, I.; Lloyd, S.; Aspuru-Guzik, A. Environment-assisted quantum transport. *New J. Phys.* **2009**, *11*, 033003.
- (52) Lewis, K. L. M.; Fuller, F. D.; Myers, J. A.; Yocum, C. F.; S. Mukamel, S.; Abramavicius, D.; Ogilvie, J. P. Simulations of the Two-Dimensional Electronic Spectroscopy of the Photosystem II Reaction Center. *J. Phys. Chem. A* **2013**, *117*, 34–41.
- (53) Zhu, J.; van Stokkum, I. H. M.; Paparelli, L.; Jones, M. R.; Groot, M. L. Early Bacteriopheophytin Reduction in Charge Separation in Reaction Centers of *Rhodobacter sphaeroides*. *Biophys. J.* **2013**, *104*, 2493–2502.
- (54) Bennett, D. I. G.; Amarnath, K.; Fleming, G. R. A structure-based model of energy transfer reveals the principles of light harvesting in photosystem II supercomplexes. *J. Am. Chem. Soc.* **2013**, *135*, 9164–9173.